Investigation of Rat Bone Material Properties via Three-point Bending Analysis

Aidan Boyne

Introduction

Quantifying the material properties of bone is essential if one hopes to understand degenerative bone diseases and develop treatments including medications and prosthetics. These properties are primarily the result of complex interactions within and between the mineral and collagen components which make up the bone [8]. In this report, the loading curve of several rat femurs which have undergone treatments to isolate both collagen and mineral components were determined via a three-point bending setup. The loading curves were then used to derive the material properties of the bone and construct a finite element model (FEM) for further analysis.

The bones tested in the three-point bending experiment were a control, unaltered rat femur, a collagen denatured rat femur, and a demineralized rat femur. Via the three-point bending, three representative material properties - the young's modulus, yield stress, and toughness - of each bone were determined. These material properties were selected as they give insight into bone behavior at both physiological and dangerous tensile loads. Before conducting the experiment, we hypothesized that the control bone would have greater values for all three parameters than either the collagen denatured or demineralized samples based on previous research by Rho et. al. [8]. We also predicted the collagen denatured sample would have a larger young's modulus and toughness than the demineralized sample, which would likely exhibit a very shallow slope its stress/strain graph.

The primary goal of the finite element models was to give a more ethical and convenient alternative to testing with rat bones. As such, the models were constructed to behave as closely to the actual bone as possible by using data obtained during the three-point bending protocol.

Two models were created: a simple hollow cylinder and a more complex model based on a micro-computerized-tomography (micro-CT) image. If the models proved to be sufficiently accurate, a variety of simulations testing out different properties and situations could be performed without the need for additional rat specimens or costly lab equipment.

Experimental Lab

Methods

The three-point bending analysis was preformed using a KIP Instron 8511 load frame set up as shown in Diagram 1. Each femur was placed into the load frame with the patellar line facing up for both stability and consistency with the geometry used in the later FEM. The outer and inner diameters of each bone were measured (with the exception of the inner diameter of the demineralized bone) and used to approximate the bending moment of inertia about the neutral axis.

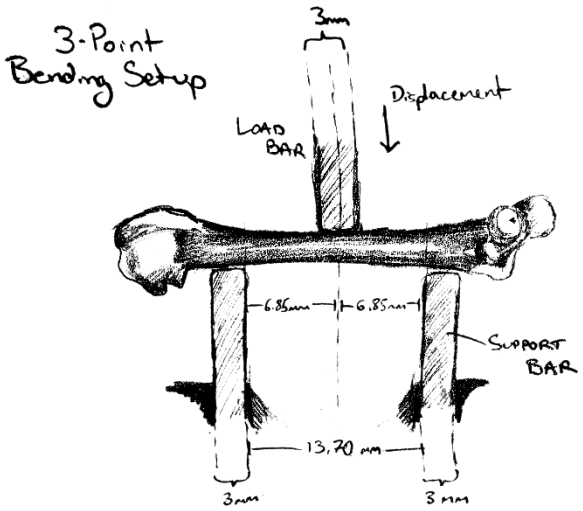

Diagram 1. A schematic illustrating the geometry of the three-point bending apparatus

During the test, the bones were preloaded at 0.1 mm/sec up to an initial resistance of 10N which was then maintained for 10 seconds. The loading bar then moved downwards at a speed of 1.0 mm/s until the bone failed or maximum displacement of the setup was reached. Running time, axial force, and axial displacement were recorded over the course of the test and used to construct a load-displacement curve.

As seen in figure 1, the demineralized sample never reached the initial resistance load of 10N, so no determination of material properties was possible. For the remaining control and collagen denatured samples, the stress and strain were calculated using the equations derived in diagram 2. These equations were derived by approximating the rat femur as a perfect hollow cylinder of uniform density using the inner and outer diameter measurements taken before and after the experiment. The young's modulus of each sample was then determined via the slope of a linear regression in the elastic region of the stress-strain curve while yield stress and toughness were found graphically.

Derivation of Bending Stress and Strain

At any point in time the problem can be treated as static such that:

$$\sum F_y = 2F_s - F_l = 0 \Rightarrow F_s = \frac{1}{2}F_l$$

$$M = F_s(L/2) \Rightarrow M = \frac{1}{4}F_l \cdot L$$

The bending moment of inertia about the neutral axis is $I = \frac{\pi}{4}(r_o^4 - r_i^4)$. Maximum bending stress σ_b occurs when $r = r_o$ so we have:

$$\sigma_b = \frac{M \cdot r_o}{I} = \frac{\frac{1}{4}F_l \cdot L}{\frac{\pi}{4}(r_o^4 - r_i^4)} = \frac{F_l \cdot L}{\pi(r_o^4 - r_i^4)}$$

Maximum bending strain will similarly occur at $r = r_o$ and can be derived using r_o, L, and displacement at the load bar δ [5]. The resulting equation is

$$\epsilon_b = \frac{12r_o \cdot \delta}{L^2}$$

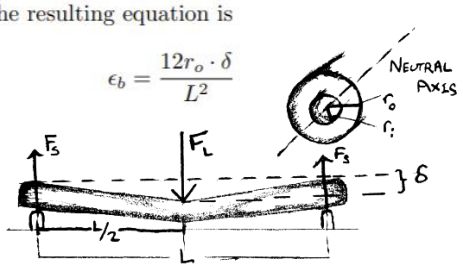

Diagram 2. Illustration of necessary measurement and equations to determine bending stress and strain

Results

Table 1. Summarized results of three-point bending test

	Young's Modulus (GPa)	Yield Stress (MPa)	Toughness (KJ/m^3)
Intact Bone	3.609	141.1	45.91
Collagen Denatured Bone	2.189	80.16	17.25

The results of the three-point bending test are shown in figure 1 and figure 2. Note that the demineralized specimen never reached the requisite preload of 10N within the maximum displacement of 8mm and was therefore excluded from stress-strain analysis.

To best approximate linear elastic behavior of the bone the line of best fit was calculated via linear regression. The slope was then multiplied by a constant modifier to match the linear region of the stress strain curve resulting in the young's moduli shown in table 1.

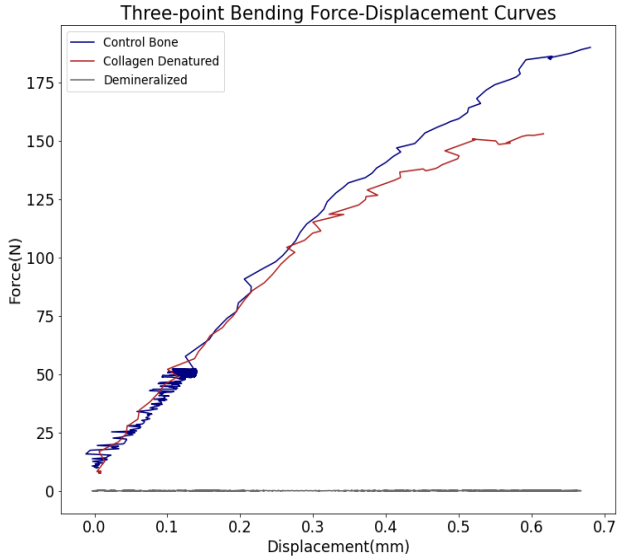

Figure 1. Displacement of the three tested specimens under increasing load. Preloading phase and any points after failure of the bone were omitted for clarity.

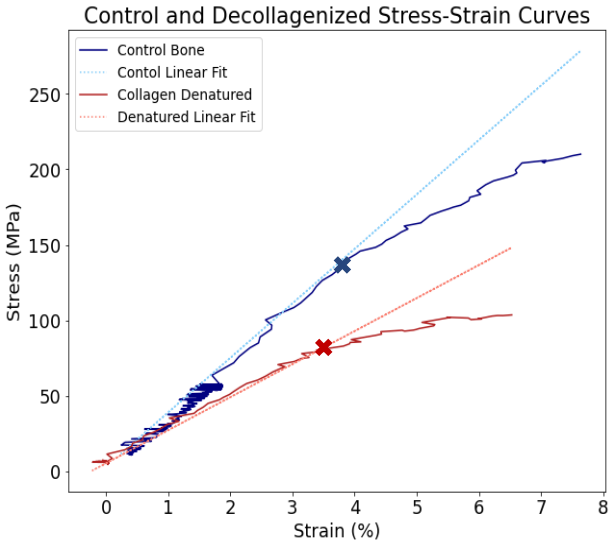

Figure 2: Stress-strain curves and lines of best fit in the elastic region calculated with weighted linear regression. Yield stress is marked with ✖ on the graph.

Discussion

At first glance, the structural properties of the control and collagen denatured bones are remarkably similar, especially in what appears to be the elastic portion of the force-displacement curve. The similarity is misleading, however, and the difference between the two samples becomes clear when the geometry of the bones (specifically the inner and outer radii of the cross sections) is taken into account through the moment of inertia about the bending axis in the stress-strain curve. As emphasized by Meulen et. al., it is always important to consider the distinction between structural (extrinsic) and material (intrinsic) properties [7]. This is especially applicable in the current analysis of the sample bones which have notable geometrical differences, and is the primary reason why material rather than structural properties were chosen for comparison.

Moving to figure 2, it is clear that the intact bone possessed the greatest young's modulus, yield stress, and toughness of the three samples as expected. The demineralized sample's almost complete lack of resistance to displacement, however, was surprising, and unfortunately no meaningful conclusions regarding its material properties could be reached and it was omitted from the figure.

The results from the demineralized bone are not completely useless, though, as they demonstrate how crucial the mineral component is to the stiffness and toughness of bone. Still, even though the collagen was unable to bear any bending load on its own, it plays an important role as illustrated by the collagen denatured sample. The denatured sample's young's modulus was almost 40% lower than that of the control and the overall toughness less than half that of the control. This marked decrease in material properties is likely due to the compromised microarchitecture and resulting lack of flexible support for the mineral crystals [4]. Without the high tensile strength of the cross-linked collagen matrix, the bone lost a significant portion of its elasticity and energy storing capacity.

The values obtained for our chosen parameters are comparable to those obtained in previous studies with intact bones. The control femur toughness of 45.91 KJ/m^3 was within the range of 30 and 60 KJ/m^3 measured by Launey et. al while the yield stress of 141.1 MPa is slightly above the average of 109 MPa obtained by Corey et. al. via uniaxial compression tests [3] [6].

The young's modulus of 3.609 GPa measured in the control femur is a bit more difficult to validate and brings up the important point of test methodology. Kuhn et. al. obtained a nearly identical value of 3.81 GPa using a three-point bending setup but other methods such as a nanoindentation test by Rho. et. al. or use of a strain gauge by Turner et. al. have obtained values as high as 19.6 ± 3.5 GPa and 29.4 GPa respectively [8] [10]. Such large discrepancies cannot be explained through sample variation and are likely due to the limitations of the respective testing methods. For example, in a three-point bending analysis, the entire bending moment is assumed to act in the in the loading direction, shear forces are ignored, and strain is overestimated due to local deformation at the loading bar. Furthermore, approximating the bone as a hollow cylinder to simplify calculations leads to small inaccuracies in the bending moment of inertia [10]. Altogether, these limitations and approximations add up and lead to the unusually wide range of values reported by different sources.

Ideally, data from a range of structural, material, and geometric analysis should be taken into account to provide an accurate and complete picture of a bone's material properties [7]. Three-point bending, however, is a relatively simple procedure which produces sufficient data to make meaningful comparisons between samples tested in the same way and is well suited to answering the questions posed by the hypothesis [9] [10]. Other methods such as the use of strain gauges could potentially provide more accurate measurements but require more exact placement and calibration which are

difficult to replicate reliably. Once sufficient data has been collected, however, it is more ethical (and potentially more efficient and cost effective) to switch to numerical models such as the finite element model constructed in the following phase of this investigation. In the meantime, the number of animals used for testing can also be reduced by using as many parts of the animal as possible – in our case the tails from the lab rats will be used in future tendon studies. Of course, those animals that must be used should be treated with respect and given adequate living conditions throughout their lifespan.

Numerical Lab

Methods

Two finite element models were constructed using the material properties obtained in the three-point bending test of the control bone. For simplicity, both models assume bone is linearly elastic and isotropic. The first model was a perfect cylinder with the same inner and outer diameters as the control bone. The cylinder model consisted of 4237 nodes connected to form a two-layered mesh of 4-node tetrahedrons. The second model was constructed using the geometry of a rat femur from a micro-CT image (note this was a different femur than the one used in the experimental test). A mesh was similarly constructed from the 6916 nodes using 4-node tetrahedrons.

In both FEMs, each node was assigned the young's modulus of 3.609 GPa derived in the experimental section and a Poisson's ratio of 0.35 based on previous literature [10].

Boundary conditions representing the supports and loading bar were modelled by restricting movement in all directions (setting a displacement of 0) at 16 nodes along each of the supports and applying a fixed displacement in the y-direction at 18 nodes along the loading bar as shown in diagram 3. The location of the nodes was selected to match the contact geometry of the experimental setup as closely as possible. Displacements of 0.30mm and 0.61mm were selected to model elastic and plastic deformations respectively. The simulated displacement was applied at the 18 loading nodes in 10 equal increments over 100ms and the resulting stresses and strains were recorded for both models. Reaction forces at the supports and load bar were also recorded for comparison with the experimental data.

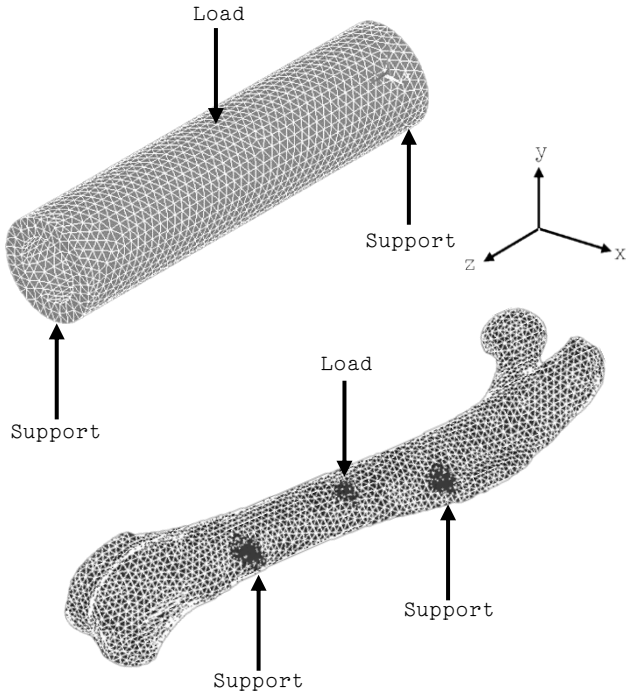

Diagram 3. Illustration of cylindrical (top) and CT-geometry (bottom) finite element models. Boundary conditions specified by arrows.

Results

Table 2. Summarized results of finite element simulations. Displacement of 0.31mm corresponds to the elastic region of the bone while displacement of 0.60mm corresponds to the plastic region according to experimental data. All stresses and strains are in the z-direction as shown in diagram 3.

Model	Displacement (mm)	Maximum Tensile Stress (MPa)	Maximum Strain (%)	Reaction Force (N)
Cylinder	0.31	52.7	2.27	108.8
Cylinder	0.6	192.8	5.63	153
CT-geometry	0.31	59.0	1.28	175.2
CT-geometry	0.6	114.2	2.48	339.1

The results of the four simulations conducted are presented in Table 2. Graphical representations of the tensile stresses for the cylinder and CT-geometry trials are depicted in figure 3. Due to assumptions of linear elasticity and isotopy, strain distribution throughout the bone is identical to that of stress and is not shown.

Figure 3. Distribution of stresses throughout the cylindrical (a,b) and CT-geometry models (c,d) under elastic and plastic deformation. High tensile stresses are positive and shown as red on the graphs while compressive stresses are negative shown as blue.

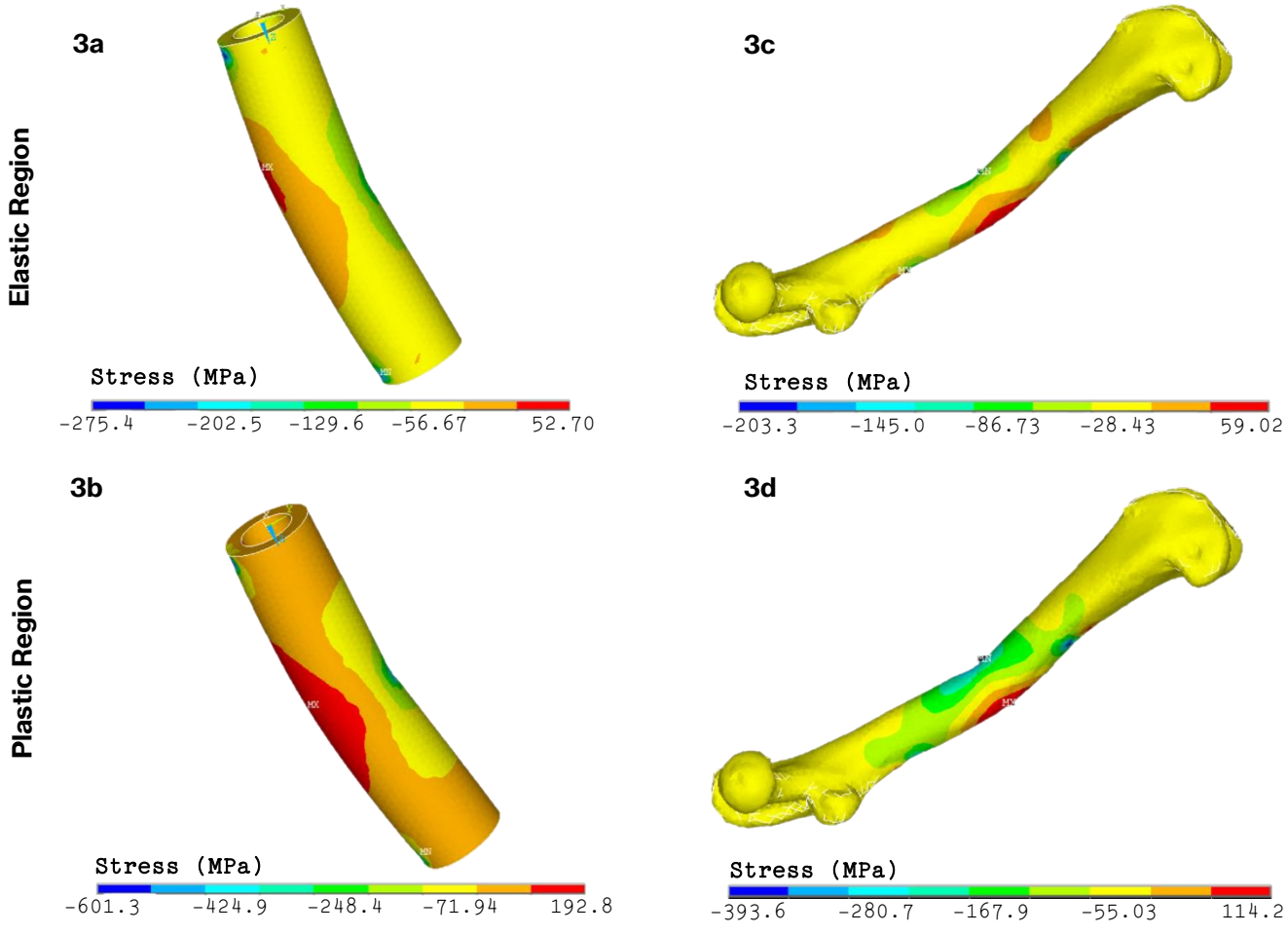

Discussion

The solutions of both the cylindrical FEM and CT-geometry FEM (CT-FEM) showed very similar distributions of stresses and strains. The maximum tensile stresses and strains in occurred at the region opposite the loading bar as expected and diminished in an elliptical pattern towards the edges of the model. Stress values in the elastic region are also similar, but there are major differences in both strain and reaction forces between the two models, especially in the post-elastic (plastic) region. One primary reason for this is that the CT-FEM was notably thicker than the cylinder model (this will be discussed in more detail later).

To confirm that the finite element models simulated the rat bones as closely as possible, reaction forces on the support beams were calculated for both the experimental results and the FEM. Boundary conditions were then adjusted until the reaction forces for the cylindrical model were accurate to ±10% of those in the experiment. The resulting cylindrical model displayed stresses and strains that agreed well with the experimental data, though absolute values for all parameters were around 20% less than those calculated experimentally. This can be at least partially explained by the assumption that all stresses and strains occurred in the loading (z) direction for the experimental model, while the FEM allowed for some stress and strain in the other directions. Furthermore, the supports in the experimental trials realistically allowed some movement due to bone slipping, while the FEM boundary conditions completely restricted the ends of the bone. This led to some inaccuracy when measuring bone displacement and explains the unrealistically large compressive stresses found at the support boundaries (see figure 3).

Using similar boundary conditions in the CT-FEM resulted in reaction forces significantly higher than those of the experimental model. This difference is predictable, however, as the CT-scan used to construct the FEM was of a different specimen which was thicker than the one used in the experimental trial. As a result, the CT-FEM had a greater bending moment of inertia and required greater load and accompanying reaction forces to achieve the same displacement as the experimental model. The greater bending moment of inertia also partially explains the lower stress and strains observed in the CT-FEM in addition to the reasons mentioned earlier for the cylindrical model which also apply here.

Altogether, the factors mentioned above resulted in a maximum strain of only 2.48% in the CT-FEM. Based on experimental observations, this is not within the plastic region of rat bone, so further refinement of the model would be advisable before use in any simulations where experimental validation is unavailable. The cylindrical model, however, produces results comparable to those in literature: take for example the average reaction forces of 106N and 142N at 0.31mm and 0.60mm recorded by Brzóska et. al. which are almost identical to those of the cylindrical model (table 3) [2].

In any FEM, some uncertainty is inevitable exactly because the model is *finite* while the real world is functionally *infinite*. Some assumptions regarding boundary conditions, geometric resolution, and the distribution of

material properties must be made for all simulations. As such, FEMs are typically a helpful supplement to understand pool of experimental data (as in this report) and rarely a replacement for the experiment itself.

Discussion

Looking at the combined results from both the experimental and FEM portions of the investigation, it is clear that the overall mechanical behavior of bone stems from both structural and material properties. For example, even though the nodes of both FEMs were assigned a young's modulus of 3.61GPa, the observed stress strain ratio was 2.32 GPa in the cylindrical model and 4.61 GPa in the CT-FEM. These findings are consistent with previous literature and emphasize the importance of both structural and material tests if one seeks to understand the whole picture of bone biomechanics [7].

Although all tests previously discussed were performed on rat bone, the results still have relevance for human applications. Human and rat bone are composed of the same hydroxyapatite and collagen matrix and have been shown to display similar mechanical behavior (after compensating for size differences) despite subtle differences in osteocyte and osteon structure [1]. In fact, rats are often used in preliminary animal studies for novel drugs for bone disorders and for implant materials [1]. Rat bone may be less appropriate for testing prostheses, however, due to postural differences and a 11° disparity in average femoral head angle [1].

Overall, the results of this study provide a solid starting point to understanding the biomechanics of bone but more data is necessary to construct a reliable finite element model. Testing the rat femurs under axial tension and compression and measuring the density at different points along the diaphysis and epiphysis would give important information for a more realistic FEM [5]. Future studies could also examine the properties of demineralized bone using alternative testing setups with larger displacement limits to give a more complete synopsis of the contributions of bone's collagen component.

References

[1] Bagi CM, Berryman E, Moalli MR. Comparative bone anatomy of commonly used laboratory animals: implications for drug discovery. *Comp Med*. 2011;61(1):76-85.

[2] Brzóska, M.M., Majewska, K. & Moniuszko-Jakoniuk, J. Mechanical Properties of Femoral Diaphysis and Femoral Neck of Female Rats Chronically Exposed to Various Levels of Cadmium. *Calcified Tissue International*. 2005;**76,** 287–298.

[3] Cory E, Nazarian A, Entezari V, Vartanians V, Müller R, Snyder BD. Compressive axial mechanical properties of rat bone as functions of bone volume fraction, apparent density and micro-ct based mineral density. *J Biomech*. 2010;43(5):953-960.

[4] Hernandez CJ, Keaveny TM. A biomechanical perspective on bone quality. *Bone*. 2006;39(6): 1173–1181.

[5] Kuhn JL, Goldstein SA, Choi KW, London M, Feldkamp LA, Matthews LS. Comparison of the trabecular and cortical tissue moduli from human iliac crests. *Journal of Orthopedic Research*. 1989;7:876–84

[6] Launey ME, Buehler MJ, Ritchie RO. On the mechanistic origins of toughness in bone. *Annual Review of Materials Research.* 2009;36(1).

[7] Meulen MCH, Jepsen KJ, Mikic B. Understanding Bone Strength: Size Isn't Everything. *Bone*. 2001;29(2):101-104.

[8] Rho JY, Kuhn-Spearing L, Zioupos P. Mechanical properties and the hierarchical structure of bone. *Medical Engineering & Physics.* 1998;20:92-102.

[9] Sharir A, Barak M, Shahar R. Whole bone mechanics and mechanical testing. *The Veterinary Journal*. 2008; 177: 8-17.

[10] Turner CH, Burr DB. Basic Biomechanical Measurements of Bone: A Tutorial. *Bone*. 1993;14:595-608.